Author/s:
Gupta, N;Kim, H;Azar, NS;Uddin, SZ;Lien, DH;Crozier, KB;Javey, A

Title:
Bright Mid-Wave Infrared Resonant-Cavity Light-Emitting Diodes Based on Black Phosphorus

Date:
2022-02-09

Citation:
Gupta, N., Kim, H., Azar, N. S., Uddin, S. Z., Lien, D. H., Crozier, K. B. & Javey, A. (2022). Bright Mid-Wave Infrared Resonant-Cavity Light-Emitting Diodes Based on Black Phosphorus. Nano Letters, 22 (3), pp.1294-1301. https://doi.org/10.1021/acs.nanolett.1c04557.

Persistent Link:
https://hdl.handle.net/11343/332901

Bright Mid-Wave Infrared Resonant-Cavity Light-Emitting Diodes Based on Black Phosphorus

Niharika Gupta, Hyungjin Kim, Nima Sefidmooye Azar, Shiekh Zia Uddin, Der-Hsien Lien, Kenneth B. Crozier, and Ali Javey*

ABSTRACT: The mid-wave infrared (MWIR) wavelength range plays a central role in a variety of applications, including optical gas sensing, industrial process control, spectroscopy, and infrared (IR) countermeasures. Among the MWIR light sources, light-emitting diodes (LEDs) have the advantages of simple design, room-temperature operation, and low cost. Owing to the low Auger recombination at high carrier densities and direct bandgap of black phosphorus (bP), it can serve as a high quantum efficiency emitting layer in LEDs. In this work, we demonstrate bP-LEDs exhibiting high external quantum efficiencies and wall-plug efficiencies of up to 4.43 and 1.78%, respectively. This is achieved by integrating the device with an Al_2O_3/Au optical cavity, which enhances the emission efficiency, and a thin transparent conducing oxide [indium tin oxide (ITO)] layer, which reduces the parasitic resistance, both resulting in order of magnitude improvements to performance.

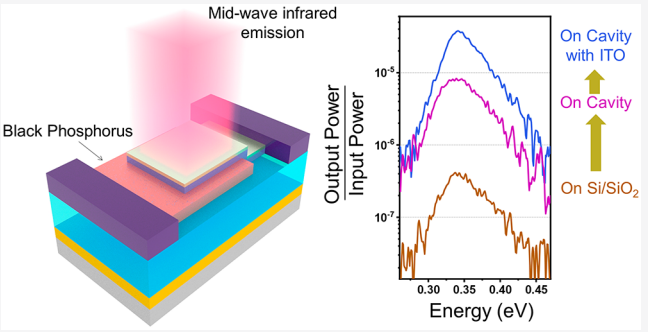

KEYWORDS: *bP, LED, two-dimensional (2D) materials, parasitic resistance, light extraction efficiency, ITO*

The mid-wave infrared spectral range (MWIR, λ = 3−8 μm), is classified as eye safe, which makes it attractive for applications including target imaging, illumination, and free-space optical communication. In addition, MWIR covers fundamental vibrational resonance bands of a wide range of materials, including water, polymers, toxic and explosive agents, and molecular gases, such as CO_2 and methane.[1] An application related to the latter, i.e., gas sensing, has been of much interest lately, e.g., for smart homes, oil and gas production, and wearable health monitoring. This growing market has motivated the development of III−V and II−VI semiconductor-based laser technologies, such as quantum-cascade lasers (QCLs), interband cascade lasers (ICLs), and quantum-well lasers. These provide high optical power and narrow spectral width but with the trade-off of system complexity and high power requirement and fabrication cost.[2] Inexpensive alternatives, such as thermal light emitters, come at the cost of broad spectral width and limited modulation frequencies.[2,3] In contrast, light-emitting diodes (LEDs) present the opportunity for low cost but also have favorable characteristics, such as brightness adjustment via pulse-width modulation and narrow spectral width.

Conventional MWIR LEDs based on III−V and II−VI semiconductors exhibit low efficiencies (even theoretically) as a result of a high Auger recombination coefficient, which is inherent to semiconductors with small bandgap and large asymmetry in carrier effective masses.[4] Therefore, there is a tremendous technological need for the development of a new emitter material in the MWIR with higher quantum yield and efficiency. Black phosphorus (bP), a two- dimensional (2D) material, has a much lower Auger recombination coefficient compared to III−V and II−VI semiconductors with similar bandgaps as a result of smaller asymmetry in effective masses, presenting an opportunity as the emitting layer for more efficient MWIR LEDs.[5−7] A lower Auger recombination coefficient leads to a higher quantum yield (QY), which is the fraction of recombination events that emit photons and is given by the ABC model as

$$QY = \frac{B(np - n_i^2)}{A(np - n_i^2)/p + B(np - n_i^2) + 2Cn(np - n_i^2)} \quad (1)$$

where A, B and C are the Shockley−Read−Hall (SRH), radiative bimolecular, and Auger recombination coefficients, respectively, and n_i and n/p are the intrinsic and total electron/hole concentrations, respectively. The bP has a much higher

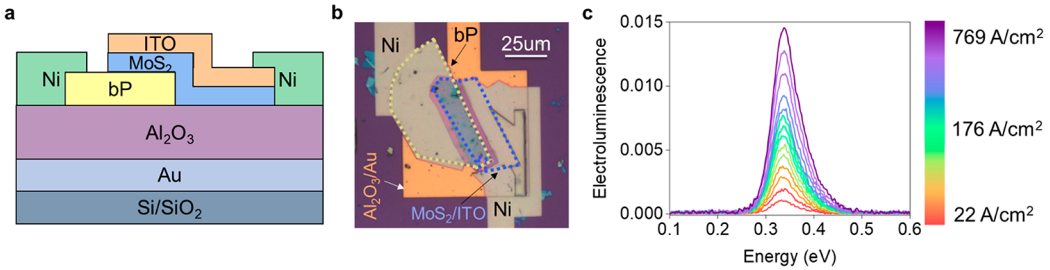

Figure 1. (a) Schematic showing the device cross section. (b) Optical micrograph of a typical device with 80 nm bP, 8 nm MoS_2, 10 nm ITO, and 360 nm Al_2O_3 layer. (c) Electroluminescence measured from the device shown in panel b as a function of the injection current density with a peak emission at 0.34 eV.

MWIR photoluminescence (PL) intensity than indium arsenide (InAs) multiple quantum well (MQW), confirming its prospects for photonic appplications.[8] Another advantage of bP is that its PL emission is linearly polarized.[9] Owing to its puckered honeycomb lattice, bP shows novel anisotropic optical, electronic, mechanical, thermal, and optical properties along the two orthogonal directions of armchair and zigzag.[10,11] Furthermore, the material shows high hole mobility, and has a direct and widely tunable thickness-dependent bandgap that ranges from 0.3 to 2 eV, a spectral region containing absorption lines of numerous gases.[12,13] This confirms the prospects of bP-based LEDs for applications involving selective sensing of gases.

The bP-LEDs investigated thus far are in the form of bP/MoS_2 heterojunctions, which have intrinsic p- and n-type characteristics, respectively, and produce MWIR electroluminescence.[14,15] It has also been shown that high output power can be achieved when the device is modified to include graphene electrodes to allow for the injection of a high current into the bP layer.[16] Even though these works have documented bP-LEDs with remarkable properties, there have not been extensive efforts to improve their external and wall-plug efficiencies. In this work, we demonstrate techniques to improve these metrics by addressing two key problems.

The first problem is that of limitations to the wall-plug efficiencies of the previously demonstrated bP-LEDs as a result of the high parasitic resistances of the materials. Even though MoS_2 forms a low Schottky barrier height with metal contacts (such as Au or Ni) for electron injection into bP, there is still considerable scope for reducing the overall resistance of the device. To shunt the lateral parasitic resistance of the MoS_2 layer, we employ a thin film of indium tin oxide (ITO). ITO has low resistivity because it is a n-type degenerate semiconductor.[17] We chose ITO rather than a metal as a result of its high optical transparency. Furthermore, mitigation of the parasitic resistance is critical for not only improving wall-plug efficiency but also extending the operating lifetime. This is because high parasitic resistances can lead to excessive device temperatures as a result of joule heating. This can contribute to melting/vaporizing/diffusing processes occurring in the device and accelerate void formation, which can ultimately lead to permanent device degradation and/or failure.[18,19]

Another issue with the bP-LED devices demonstrated thus far is that a large fraction of the generated photons is lost via either emission through the bottom side or total internal reflection, while only the extracted optical power determines the overall device performance. To improve the light extraction efficiency in conventional LEDs, various methods, including die shaping,[20,21] textured semiconductor surfaces,[22,23] contact geometries,[24,25] anti-reflection optical coatings,[26] transparent contacts,[27] flip-chip packaging,[28−30] and resonant cavities,[31−33] have been employed. In particular, resonant cavities result in not only an enhanced light outcoupling but also a more directed far-field emission pattern, which makes resonant-cavity light-emitting diodes (RC-LEDs) desirable for optical communication systems.[34] Optical cavities have also been employed for enhancing the light absorption and, thus, photodetection performance of 2D materials.[35,36] In this study, an optical cavity consisting of gold and Al_2O_3 films was formed under the light-emitting bP/MoS_2 heterojunction such that the emission couples to the resonant mode of the cavity, and therefore, enhances the emission efficiency of the bP-based LEDs.

A schematic of the cross section and an optical microscope image of the device are shown in panels a and b of Figure 1, respectively. The fabrication process is discussed in section S1 of the Supporting Information, and bP characterization with Raman spectroscopy is presented in section S2 of the Supporting Information. The bP flakes with thicknesses of 40 ± 5 nm and MoS_2 flakes with thicknesses of 8 ± 2 nm were used in all experiments. This results in an emission peak at ∼0.34 eV (λ = 3.65 μm) in our bP-LEDs with a full width at half maximum (fwhm) of ∼0.7 μm. Using bP flakes with appropriate thickness is important here, because its bandgap is strongly modulated by thickness. The bandgap of MoS_2 remains constant at 1.29 eV for bulk thicknesses.[37] Typical emission spectra measured at different injection current densities are shown in Figure 1c. These spectra were collected using a double-modulated lock-in detection technique, as described in section S3 of the Supporting Information. The electroluminescence intensity increases with a higher current injection density without any change in the peak energy. This confirms that the emission originates from the bP band edge recombination. The characterization of the polarized emission from the LED is shown in section S4 of the Supporting Information.

The Al_2O_3/Au optical cavity was designed using optical simulations. For an emitter with a low intrinsic quantum efficiency, the emission enhancement factor provided by an optical structure can be expressed as $f_P\eta_{oc}$, where f_P is the Purcell factor (i.e., spontaneous emission rate enhancement provided by the optical medium) and η_{oc} is the outcoupling efficiency (i.e., fraction of radiated photons that escape the optical structure and reach the upper half-space where they are collected).[38] The Al_2O_3/Au cavity can contribute to the emission enhancement through both of these factors. In the presence of the optical cavity, the portion of the emitted light traveling downward becomes reflected from the mirror and

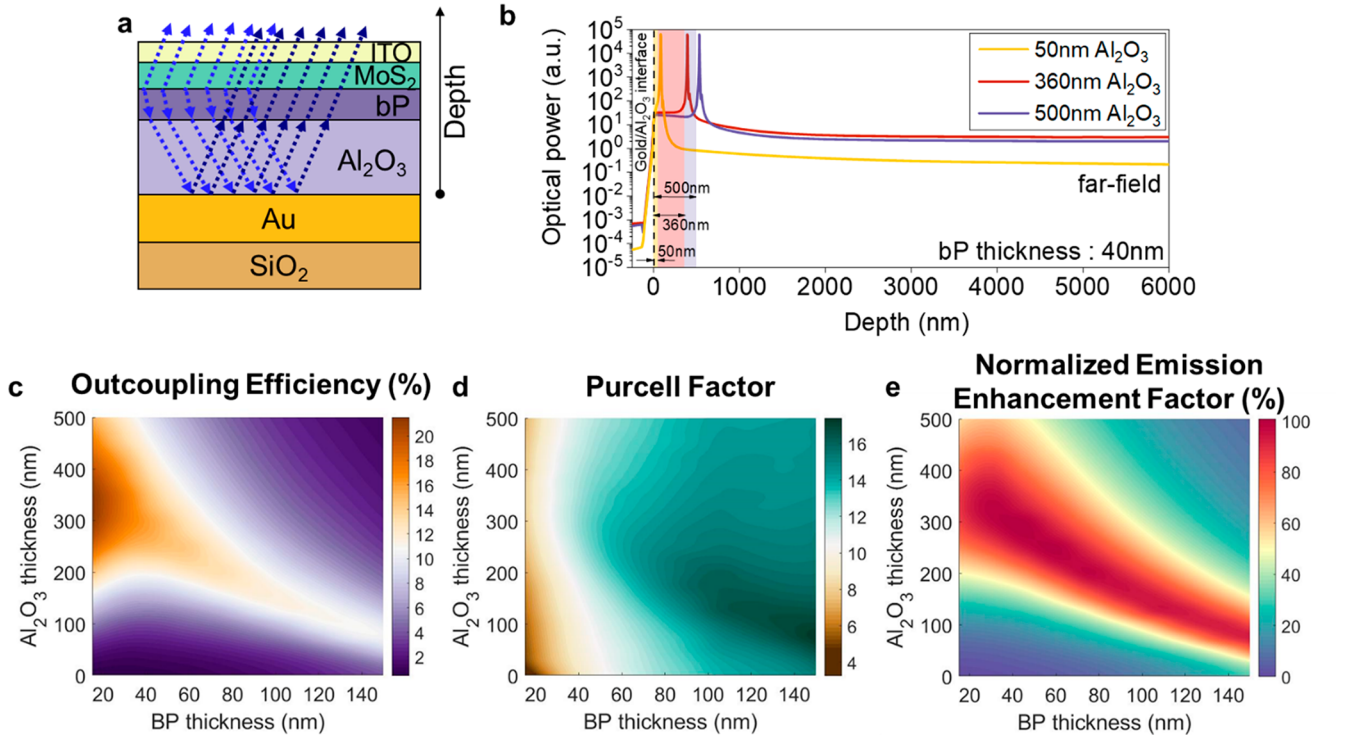

Figure 2. (a) Schematic of the device cross section showing the constructive interference of emitted light as a result of the optical cavity. (b) Simulated vertical profile of the optical power for Al_2O_3 thicknesses of 50, 360, and 500 nm for a fixed bP thickness of 40 nm. Optical simulations showing the (c) outcoupling efficiency, (d) Purcell factor, and (e) normalized emission enhancement factor variation for the device structure as a function of bP and Al_2O_3 thickness for a MoS_2 thickness of 8 nm and an ITO thickness of 10 nm.

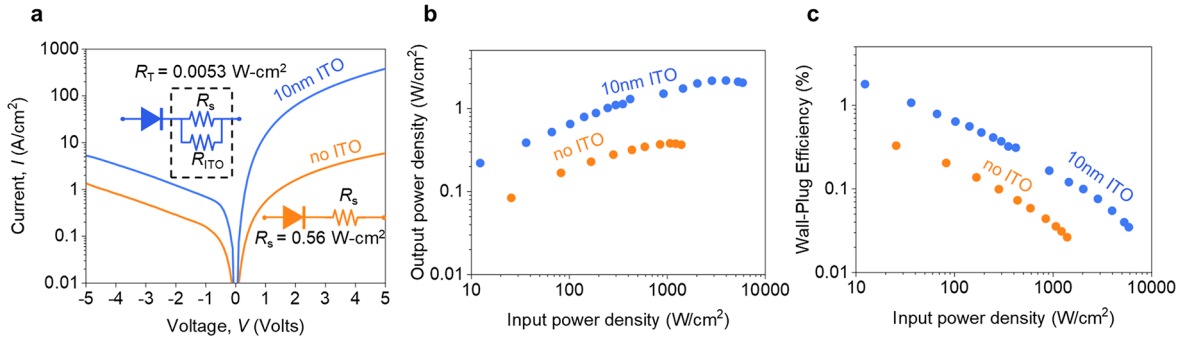

Figure 3. (a) $I-V$ characteristic and extracted series resistance for devices with and without a 10 nm thick ITO film. (b) Output power density and (c) wall-plug efficiency as functions of the input power density for LEDs with and without a 10 nm thick ITO film.

interferes with the emitted light from bP. For the interference to be constructive, the spacer thickness should be $\sim\lambda/(4n_s)$, where n_s is the refractive index of the Al_2O_3 spacer layer and λ is the wavelength of the emitted photons. Hence, the optical cavity with a proper spacer thickness enhances the outcoupling efficiency by redirecting the emitted light to the upper half-space, where it can be collected. This is schematically illustrated in Figure 2a. Figure 2b shows the optical power variation along the depth of the device for Al_2O_3 thicknesses of 50, 360, and 500 nm at $\lambda = 3.65$ μm. The simulation details are discussed in section S5 of the Supporting Information. It can be seen that a spacer thickness of 360 nm leads to the highest light outcoupling and, thus, far-field optical power. Figure 2c plots the outcoupling efficiency as functions of Al_2O_3 and bP thicknesses at fixed thicknesses of 10 nm ITO and 8 nm MoS_2. For bP thicknesses smaller than 50 nm (on a 325 nm Al_2O_3/Au cavity), the outcoupling efficiency is enhanced by more than ~50 times compared to the case without an Al_2O_3 spacer. While the outcoupling efficiency of this structure reaches its maximum value of ~21% for bP thickness of 20 nm, the Purcell factor is not the highest in this range of bP and Al_2O_3 thickness. As illustrated in Figure 2d, the Purcell factor is greater at an Al_2O_3 thickness of ~100 nm and bP thickness of 100–150 nm. Figure 2e plots the normalized emission enhancement factor $(f_p\eta_{oc})$ as functions of Al_2O_3 and bP thicknesses. The bP films used in the experiments were 40 nm thick. Accordingly, an Al_2O_3 thickness of 360 nm should be chosen to maximize the emission enhancement factor. The comparison of optical power for different bP thicknesses at the injection current density of 50 A cm^{-2} on a 360 nm thick Al_2O_3/Au cavity is shown in section S6 of the Supporting Information. It should be noted that the optical behavior of ITO depends upon the material defect density and, thus, sputtering conditions.[39,40] Thus, the refractive index values of

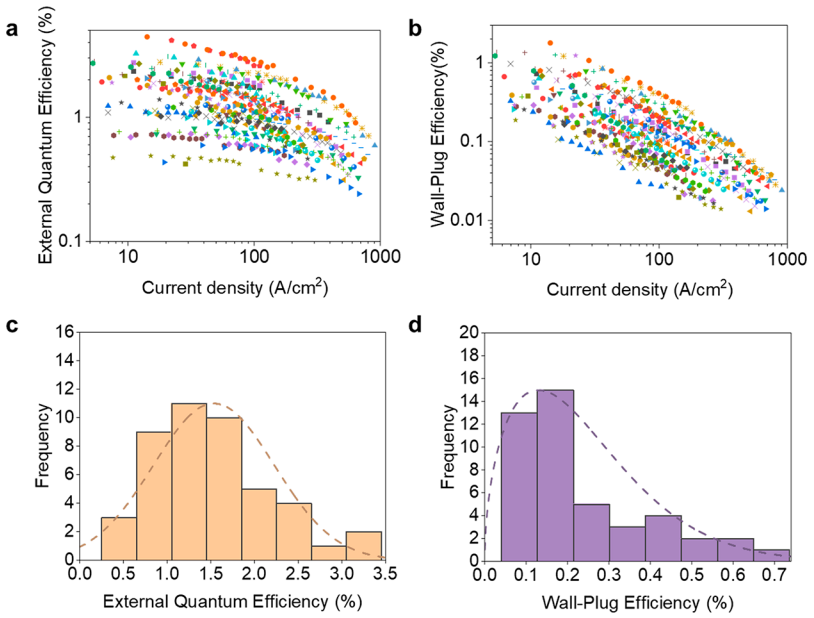

Figure 4. (a) External quantum efficiency and (b) wall-plug efficiency as functions of the input current density plotted for 45 devices fabricated with constant MoS_2, bP, ITO, and Al_2O_3 thicknesses (8, 40, 10, and 360 nm, respectively). Histograms of (c) external quantum efficiency and (d) wall-plug efficiency with Gaussian and Weibull fits, respectively, at the current density of 50 A cm^{-2}.

ITO to be used in the simulations were determined for our specific deposition parameters, as described in section S7 of the Supporting Information.

To reduce the parasitic resistance, we employed a 10 nm thick ITO layer, which has a relatively low sheet resistance of 300 Ω/sq. The effect can be quantified by comparing current−voltage (I-V) characteristics of devices with and without ITO, as shown in Figure 3a. These devices have similar junction areas of 353 μm^2 (with ITO) and 424 μm^2 (without ITO). For large forward-bias voltages, where series resistance becomes important, the current per unit junction area for the device with ITO is higher by more than an order of magnitude compared to the device without ITO. The forward-bias series resistance is evaluated using the following method.[34] The diode is assumed to have a very high parallel resistance ($R_P \rightarrow \infty$), yielding the following forward-bias I−V relation:

$$I = I_S \exp\left(\frac{q(V - IR_S)}{n_{ideal}kT}\right) \tag{2}$$

where I_S is the reverse-bias saturation current, R_S is the series resistance, n_{ideal} is the ideality factor, k is the Boltzmann constant, q is the electric charge on an electron, and T is the absolute temperature of the diode. Equation 2 leads us to

$$\frac{dV}{dI} = R_S + \frac{n_{ideal}kT}{q}\frac{1}{I} \tag{3}$$

The slope of the plot of IdV/dI versus I (section S8 of the Supporting Information) is then used to determine R_S, which is 0.0053 and 0.56 Ω cm^2 and for devices with and without ITO, respectively. Hence, an about 2 orders of magnitude reduction in series resistance is achieved.

The reduction in parasitic resistance via the ITO layer improves the maximum output power density and power efficiency of the device. The output optical power from the device was determined using the calibration method discussed in section S9 of the Supporting Information. Figure 3b shows that the device with a 10 nm thick ITO layer produces a maximum optical power of 2.2 W/cm^2, which is more than 5 times higher than that for the device without ITO, i.e., 0.4 W/cm^2. Despite having a slightly lower photon extraction efficiency, the device with ITO shows higher brightness per unit area. This can be attributed to the reduction in series resistance achieved via the ITO layer, which improves the voltage drop across the device.

The LED with low parasitic resistance outperforms the device without ITO in terms of power efficiency as well, as shown in Figure 3c. This is also called wall-plug efficiency (η_{power}) and is the ratio of the total detected optical power (P) to the total input electrical power injected into the device

$$\eta_{power} = \frac{\text{detected optical power}}{\text{input electrical power}} = \frac{P}{IV} \tag{4}$$

The device with ITO achieves a wall-plug efficiency of 0.3% at an input power density of 418 W/cm^2, while for the device without ITO, the wall-plug efficiency is 0.07% at a (similar) input power density of 435 W/cm^2.

The output power density increases sub-linearly with input power density according to the "efficiency-droop" effect; i.e., external quantum efficiency (η_{EQE}) is reduced as a result of Auger recombination at higher carrier densities.[41,42] η_{EQE} is defined as the ratio between the number of detected photons and the number of electrons injected into the device

$$\eta_{EQE} = \frac{\text{number of detected photons}}{\text{number of injected electrons}} = \frac{P/(hc/\lambda)}{I/q} \tag{5}$$

where h is Planck's constant, c is the speed of light, and λ is the wavelength of the emitted photons. For devices with and without a 10 nm ITO layer, the output power density saturates at input power densities of ∼3000 and 1000 W/cm^2, respectively, and it starts drooping with increasing input power. It is anticipated that the junction temperature plays a significant role here, because Auger recombination coefficients increase exponentially with increasing temperature[43] and no

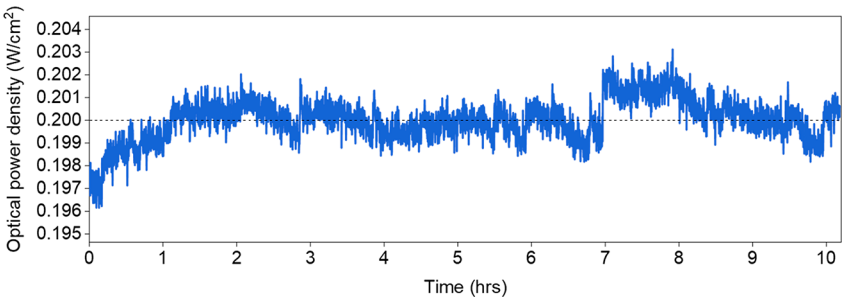

Figure 5. Drift of optical power density measured for a duration of 10 h at a modulation frequency of 1 kHz, injection current density of 20.4 A/cm^2, and output power of ~0.2 W/cm^2. The dotted line shows the mean of the signal.

Table 1. Benchmark Comparison of the bP-LED Demonstrated in This Work with the State-of-the-Art MWIR Light Emitters

material system	technology	wavelength (μm)	maximum optical power density (W/cm^2)	peak η_{EQE} (%)	reference
bP-LED	LED	3.65	2.17	4.43	this work
InAs	LED	3.3	3.14	0.44	44
CdHgTe	LED	3.2	0.97	0.02	45
InAsSb	LED	4.3	0.32	0.35	46
GaInAsSb	LED	2.34	0.4	2.5	47
InAs/GaInSb/InAs	interband cascade	3.8	2.4	0.65	48
InAs/GaInSb/InAs	interband cascade	3.8	2	3.1	49
InGaAs/AlInAs	quantum cascade	3.56	857	95.7	50
InGaAs/AlInAs	quantum cascade	3.5	139	10	51
Hamamatsu L13454	LED	3.9	0.6	0.9	52
Boston Electronics LED38TO8TEC	LED	3.8	0.2	0.1	53
Thorlabs LED3800W	LED	3.8	1.5	0.2	54

temperature control mechanism (e.g., heat sinking or thermoelectric cooling) is implemented here. This results in further deterioration of external quantum efficiency (and, consequently, the output power) at higher input powers. Therefore, a possible rationale for the delayed onset of droop in devices with ITO is the lower junction temperature compared to devices without ITO. The dramatic decrease in the wall-plug efficiency with an increasing input power also originates from the reduced external quantum efficiency. While the ITO layer reduces the parasitic resistance of MoS_2, it does not affect the parasitic resistance of bP and the contact resistance.

Next, we performed a statistical study on 45 devices to determine the device-to-device variations. The results are presented in Figure 4. The "efficiency-droop" effect can be clearly observed in Figure 4a, with the peak external quantum efficiency of the champion device being 4.43% at the input current density of 14 A cm^{-2} and reducing to 0.90% at the current density of 638 A cm^{-2}. The corresponding output power densities at these current densities are 0.22 and 2.04 W/cm^2, respectively. The maximum output power density recorded from this device with an area of 353 μm^2 is 2.17 W/cm^2 (i.e., output power = 7.68 μW) at an injected carrier density of 6.2 × 10^{21} cm^{-2}. The device with the lowest peak external quantum efficiency of 0.49% at the current density of 15 A cm^{-2} exhibits a wall-plug efficiency of 0.15%, as shown in Figure 4b. Its maximum output power is 2.21 μW, achieved at an input current density of 304 A cm^{-2}. The highest wall-plug efficiency among the 45 devices (i.e., for the champion device) is 1.78%, achieved at a current density of 14 A cm^{-2}. This device exhibits a power efficiency of 0.035% at the highest injected current density of 638 A cm^{-2}.

Histograms of the external quantum efficiency and wall-plug efficiency of the 45 devices are presented in panels c and d of Figure 4, respectively. For fair comparison, the performance of the devices is evaluated at the same injection current density (of 50 A cm^{-2}), which is done through interpolation. The histogram of the external quantum efficiency follows a normal distribution with a mean of ~1.5%, as shown in Figure 4c. The minimum and maximum quantum efficiencies are 0.45 and 3.33%, respectively. The histogram of the wall-plug efficiency, as shown in Figure 4d, follows a Weibull distribution with a shape value of less than 3 (right-skewed) and a peak at ~0.17%. The minimum and maximum power efficiencies are 0.05 and 0.70%, respectively. This variability is attributed to the minor differences in the thicknesses of the layers (which modifies the extraction efficiency) and air exposure of bP during fabrication.

Figure 5 presents the drift characteristics of a test device. It shows a maximum variation of less than 2% from the mean signal in the measurement period of more than 10 h, indicating high stability. Finally, the performance of our bP-LEDs is benchmarked against the state-of-the-art MWIR light sources, such as LEDs, interband, and quantum cascade lasers, having emission wavelengths in the range of 2−4.3 μm. As shown in Table 1, our bP-LED outperforms the LEDs based on conventional material systems in terms of maximum optical power density (W/cm^2) and peak η_{EQE} (%) at room temperature. Although lagging behind the highly efficient quantum cascade laser technology, our device exhibits higher external quantum efficiency than commercially available LEDs and shows an overall comparable performance to interband cascade lasers.

In conclusion, we have demonstrated a bright and efficient electroluminescent MWIR light emitter based on bP. This is accomplished by leveraging the low Auger recombination rate in bP, an Al_2O_3/Au optical cavity to enhance the photon

extraction, and a thin transparent and conductive ITO layer to reduce the high n-side parasitic resistances. We suggest several topics for future work. Investigation of diode failure mechanisms would help to improve the injectable power and, thus, the maximum optical power. Strategies to encapsulate air-sensitive bP with oxides, 2D materials, and organics should be investigated and may further enhance the long-term stability of the device.[55,56] Studies on tuning the bP bandgap via strain engineering,[7,57] designing optical coupling structures, such as nano-antennas, for light emission enhancement,[38] and designing waveguides for integration with silicon photonic platforms[16] would help advance bP-LEDs for real-world applications. The device performance may also be improved via better alternative electron contacts to MoS_2, electrical/chemical doping,[58] double heterostructure,[59] and other high extraction efficiency designs.[60] The future works on these topics can be rewarding as a result of the potential of bP-LEDs to serve as the next-generation MWIR sources.

ASSOCIATED CONTENT

Supporting Information

The Supporting Information is available free of charge at https://pubs.acs.org/doi/10.1021/acs.nanolett.1c04557.

Fabrication of bP-LED (section S1), Raman spectroscopy (section S2), device electrical and optical measurements (section S3), polarized electroluminescence (section S4), optical simulation setup (section S5), effect of bP thickness on the optical power (section S6), ITO refractive index estimation (section S7), series resistance calculation (section S8), and calibration of the output power (section S9) (PDF)

AUTHOR INFORMATION

Corresponding Author

Ali Javey − *Electrical Engineering & Computer Sciences, University of California, Berkeley, Berkeley, California 94720, United States; Materials Sciences Division, Lawrence Berkeley National Laboratory, Berkeley, California 94720, United States;* orcid.org/0000-0001-7214-7931; Email: ajavey@berkeley.edu

Authors

Niharika Gupta − *Electrical Engineering & Computer Sciences, University of California, Berkeley, Berkeley, California 94720, United States; Materials Sciences Division, Lawrence Berkeley National Laboratory, Berkeley, California 94720, United States;* orcid.org/0000-0002-1053-5821

Hyungjin Kim − *Electrical Engineering & Computer Sciences, University of California, Berkeley, Berkeley, California 94720, United States; Materials Sciences Division, Lawrence Berkeley National Laboratory, Berkeley, California 94720, United States*

Nima Sefidmooye Azar − *Department of Electrical and Electronic Engineering and Australian Research Council (ARC) Centre of Excellence for Transformative Meta-Optical Systems, University of Melbourne, Parkville, Victoria 3010, Australia;* orcid.org/0000-0002-3263-7044

Shiekh Zia Uddin − *Electrical Engineering & Computer Sciences, University of California, Berkeley, Berkeley, California 94720, United States; Materials Sciences Division, Lawrence Berkeley National Laboratory, Berkeley, California 94720, United States;* orcid.org/0000-0002-1265-9940

Der-Hsien Lien − *Electrical Engineering & Computer Sciences, University of California, Berkeley, Berkeley, California 94720, United States; Materials Sciences Division, Lawrence Berkeley National Laboratory, Berkeley, California 94720, United States*

Kenneth B. Crozier − *Department of Electrical and Electronic Engineering, Australian Research Council (ARC) Centre of Excellence for Transformative Meta-Optical Systems, and School of Physics, University of Melbourne, Parkville, Victoria 3010, Australia;* orcid.org/0000-0003-0947-001X

Complete contact information is available at: https://pubs.acs.org/10.1021/acs.nanolett.1c04557

Author Contributions

Hyungjin Kim, Shiekh Zia Uddin, and Der-Hsien Lien contributed to the calibration process. Niharika Gupta, Nima Sefidmooye Azar, and Shiekh Zia Uddin performed the optical simulations. Niharika Gupta carried out the fabrication and measurements. All authors discussed the results and wrote the paper.

Funding

The work at Berkeley was funded by the U.S. Department of Energy, Office of Science, Office of Basic Energy Sciences, Materials Sciences and Engineering Division under Contract DE-AC02-05-CH11231 (EMAT Program KC1201). The work at Melbourne was supported by the Australian Research Council (ARC) Centre of Excellence for Transformative Meta-Optical Systems (Project ID CE200100010) and the ARC Discovery Projects Scheme (DP210103428).

Notes

The authors declare no competing financial interest.

ACKNOWLEDGMENTS

Niharika Gupta thanks Wenbo Ji, Chunsong Zhao, Vivian Wang, Naoki Higashitarumizu, and James Bullock for fruitful discussions.

REFERENCES

(1) Soref, R. Mid-infrared photonics in silicon and germanium. *Nat. Photonics* **2010**, *4* (8), 495−497.

(2) Jung, D.; Bank, S.; Lee, M. L.; Wasserman, D. Next-generation mid-infrared sources. *J. Opt.* **2017**, *19* (12), 123001.

(3) Stanley, R. Plasmonics in the mid-infrared. *Nat. Photonics* **2012**, *6* (7), 409−411.

(4) Haug, A. Auger recombination in direct-gap semiconductors: Band-structure effects. *J. Phys. C: Solid State Phys.* **1983**, *16* (21), 4159.

(5) Ge, S.; Li, C.; Zhang, Z.; Zhang, C.; Zhang, Y.; Qiu, J.; Wang, Q.; Liu, J.; Jia, S.; Feng, J.; Sun, D. Dynamical evolution of anisotropic response in black phosphorus under ultrafast photoexcitation. *Nano Lett.* **2015**, *15* (7), 4650−4656.

(6) Bhaskar, P.; Achtstein, A. W.; Vermeulen, M. J.; Siebbeles, L. D. Radiatively dominated charge carrier recombination in black phosphorus. *J. Phys. Chem. C* **2016**, *120* (25), 13836−13842.

(7) Kim, H.; Uddin, S. Z.; Lien, D.-H.; Yeh, M.; Azar, N. S.; Balendhran, S.; Kim, T.; Gupta, N.; Rho, Y.; Grigoropoulos, C. P.; Crozier, K. B.; Javey, A. Actively variable-spectrum optoelectronics with black phosphorus. *Nature* **2021**, *596* (7871), 232−237.

(8) Chen, C.; Chen, F.; Chen, X.; Deng, B.; Eng, B.; Jung, D.; Guo, Q.; Yuan, S.; Watanabe, K.; Taniguchi, T.; Lee, M. L.; Xia, F. Bright mid-infrared photoluminescence from thin-film black phosphorus. *Nano Lett.* **2019**, *19* (3), 1488−1493.

(9) Wang, X.; Jones, A. M.; Seyler, K. L.; Tran, V.; Jia, Y.; Zhao, H.; Wang, H.; Yang, L.; Xu, X.; Xia, F. Highly anisotropic and robust

excitons in monolayer black phosphorus. *Nat. Nanotechnol.* **2015**, *10* (6), 517−521.
(10) Tao, J.; Shen, W.; Wu, S.; Liu, L.; Feng, Z.; Wang, C.; Hu, C.; Yao, P.; Zhang, H.; Pang, W.; Duan, X.; Liu, J.; Zhou, C.; Zhang, D. Mechanical and electrical anisotropy of few-layer black phosphorus. *ACS Nano* **2015**, *9* (11), 11362−11370.
(11) Luo, Z.; Maassen, J.; Deng, Y.; Du, Y.; Garrelts, R. P.; Lundstrom, M. S; Ye, P. D.; Xu, X. Anisotropic in-plane thermal conductivity observed in few-layer black phosphorus. *Nat. Commun.* **2015**, *6* (1), 8572.
(12) Kim, J.; Baik, S. S.; Ryu, S. H.; Sohn, Y.; Park, S.; Park, B.-G.; Denlinger, J.; Yi, Y.; Choi, H. J.; Kim, K. S. Observation of tunable band gap and anisotropic Dirac semimetal state in black phosphorus. *Science* **2015**, *349* (6249), 723−726.
(13) Chen, C.; Lu, X.; Deng, B.; Chen, X.; Guo, Q.; Li, C.; Ma, C.; Yuan, S.; Sung, E.; Watanabe, K.; Taniguchi, T.; Yang, L.; Xia, F. Widely tunable mid-infrared light emission in thin-film black phosphorus. *Sci. Adv.* **2020**, *6* (7), No. eaay6134.
(14) Wang, J.; Rousseau, A.; Yang, M.; Low, T.; Francoeur, S.; Kéna-Cohen, S. Mid-infrared polarized emission from black phosphorus light-emitting diodes. *Nano Lett.* **2020**, *20* (5), 3651−3655.
(15) Zong, X.; Hu, H.; Ouyang, G.; Wang, J.; Shi, R.; Zhang, L.; Zeng, Q.; Zhu, C.; Chen, S.; Cheng, C.; Wang, B.; Zhang, H.; Liu, Z.; Huang, W.; Wang, T.; Wang, L.; Chen, X. Black phosphorus-based van der Waals heterostructures for mid-infrared light-emission applications. *Light: Sci. Appl.* **2020**, *9* (1), 114.
(16) Chang, T.-Y.; Chen, Y.; Luo, D.-I.; Li, J.-X.; Chen, P.-L.; Lee, S.; Fang, Z.; Li, W.-Q.; Zhang, Y.-Y.; Li, M.; Majumdar, A.; Liu, C.-H. Black phosphorus mid-infrared light-emitting diodes integrated with silicon photonic waveguides. *Nano Lett.* **2020**, *20* (9), 6824−6830.
(17) Li, S.; Tian, M.; Gao, Q.; Wang, M.; Li, T.; Hu, Q.; Li, X.; Wu, Y. Nanometre-thin indium tin oxide for advanced high-performance electronics. *Nat. Mater.* **2019**, *18* (10), 1091−1097.
(18) Meneghini, M.; Tazzoli, A.; Butendeich, R.; Hahn, B.; Meneghesso, G.; Zanoni, E. Soft and hard failures of InGaN-based LEDs submitted to electrostatic discharge testing. *IEEE Electron Device Lett.* **2010**, *31* (6), 579−581.
(19) Huang, J. J.; Kuo, H. C.; Shen, S. C. *Nitride Semiconductor Light-Emitting Diodes (LEDs): Materials, Technologies, and Applications*; Woodhead Publishing: Sawston, U.K., 2017; pp 450−452.
(20) Krames, M. R.; Ochiai-Holcomb, M.; Hofler, G. E.; Carter-Coman, C.; Chen, E. I.; Tan, I.-H.; Grillot, P.; Gardner, N. F.; Chui, H. C.; Huang, J.-W.; Stockman, S. A.; Kish, F. A.; Craford, M. G.; Tan, T. S.; Kocot, C. P.; Hueschen, M.; Posselt, J.; Loh, B.; Sasser, G.; Collins, D. High-power truncated-inverted-pyramid $(Al_xGa_{1-x})_{0.5}In_{0.5}P$/GaP light-emitting diodes exhibiting >50% external quantum efficiency. *Appl. Phys. Lett.* **1999**, *75* (16), 2365−2367.
(21) Zhang, Y.; Meng, R.; Zhang, Z. H.; Shi, Q.; Li, L.; Liu, G.; Bi, W. Effects of inclined sidewall structure with bottom metal air cavity on the light extraction efficiency for AlGaN-based deep ultraviolet light-emitting diodes. *IEEE Photonics J.* **2017**, *9* (5), 1−9.
(22) Schnitzer, I.; Yablonovitch, E.; Caneau, C.; Gmitter, T. J.; Scherer, A. 30% external quantum efficiency from surface textured, thin-film light-emitting diodes. *Appl. Phys. Lett.* **1993**, *63* (16), 2174−2176.
(23) Green, M. A.; Zhao, J.; Wang, A.; Reece, P. J.; Gal, M. Efficient silicon light-emitting diodes. *Nature* **2001**, *412* (6849), 805−808.
(24) Guo, X.; Li, Y. L.; Schubert, E. F. Efficiency of GaN/InGaN light-emitting diodes with interdigitated mesa geometry. *Appl. Phys. Lett.* **2001**, *79* (13), 1936−1938.
(25) Khan, A.; Balakrishnan, K.; Katona, T. Ultraviolet light-emitting diodes based on group three nitrides. *Nat. Photonics* **2008**, *2* (2), 77−84.
(26) Kim, J. K.; Chhajed, S.; Schubert, M. F.; Schubert, E. F.; Fischer, A. J.; Crawford, M. H.; Cho, J.; Kim, H.; Sone, C. Light-extraction enhancement of GaInN light-emitting diodes by graded-refractive-index indium tin oxide anti-reflection contact. *Adv. Mater.* **2008**, *20* (4), 801−804.
(27) Ji, C.; Liu, D.; Zhang, C.; Guo, L. J. Ultrathin-metal-film-based transparent electrodes with relative transmittance surpassing 100%. *Nat. Commun.* **2020**, *11* (1), 3367.
(28) Shchekin, O. B.; Epler, J. E.; Trottier, T. A.; Margalith, T.; Steigerwald, D. A.; Holcomb, M. O.; Martin, P. S.; Krames, M. R. High performance thin-film flip-chip InGaN−GaN light-emitting diodes. *Appl. Phys. Lett.* **2006**, *89* (7), 071109.
(29) Wierer, J. J.; Steigerwald, D. A.; Krames, M. R.; O'Shea, J. J.; Ludowise, M. J.; Christenson, G.; Shen, Y.-C.; Lowery, C.; Martin, P. S.; Subramanya, S.; Gotz, W.; Gardner, N. F.; Kern, R. S.; Stockman, S. A. High-power AlGaInN flip-chip light-emitting diodes. *Appl. Phys. Lett.* **2001**, *78* (22), 3379−3381.
(30) Kish, F. A.; Steranka, F. M.; DeFevere, D. C.; Vanderwater, D. A.; Park, K. G.; Kuo, C. P.; Osentowski, T. D.; Peanasky, M. J.; Yu, J. G.; Fletcher, R. M.; Steigerwald, D. A.; Craford, M. G.; Robbins, V. M. Very high-efficiency semiconductor wafer-bonded transparent-substrate $(Al_xGa_{1-x})_{0.5}In_{0.5}P$/GaP light-emitting diodes. *Appl. Phys. Lett.* **1994**, *64* (21), 2839−2841.
(31) Schubert, E. F.; Hunt, N. E. J.; Micovic, M.; Malik, R. J.; Sivco, D. L.; Cho, A. Y.; Zydzik, G. J. Highly efficient light-emitting diodes with microcavities. *Science* **1994**, *265* (5174), 943−945.
(32) Lee, J.; Han, T.-H.; Park, M.-H.; Jung, D. Y.; Seo, J.; Seo, H.-K.; Cho, H.; Kim, E.; Chung, J.; Choi, S.-Y.; Kim, T.-S.; Lee, T.-W.; Yoo, S. Synergetic electrode architecture for efficient graphene-based flexible organic light-emitting diodes. *Nat. Commun.* **2016**, *7* (1), 11791.
(33) Schubert, E. F.; Wang, Y. H.; Cho, A. Y.; Tu, L. W.; Zydzik, G. J. Resonant cavity light-emitting diode. *Appl. Phys. Lett.* **1992**, *60* (8), 921−923.
(34) Schubert, E. F. *Light-Emitting Diodes*; Cambridge University Press: Cambridge, U.K., 2006; pp 64−256.
(35) Sefidmooye Azar, N.; Bullock, J.; Shrestha, V. R.; Balendhran, S.; Yan, W.; Kim, H.; Javey, A.; Crozier, K. B. Long-Wave Infrared Photodetectors Based on 2D Platinum Diselenide atop Optical Cavity Substrates. *ACS Nano* **2021**, *15* (4), 6573−6581.
(36) Amani, M.; Tan, C.; Zhang, G.; Zhao, C.; Bullock, J.; Song, X.; Kim, H.; Shrestha, V. R.; Gao, Y.; Crozier, K. B.; Scott, M.; Javey, A. Solution-synthesized high-mobility tellurium nanoflakes for short-wave infrared photodetectors. *ACS Nano* **2018**, *12* (7), 7253−7263.
(37) Mak, K. F.; Lee, C.; Hone, J.; Shan, J.; Heinz, T. F. Atomically thin MoS_2: A new direct-gap semiconductor. *Phys. Rev. Lett.* **2010**, *105* (13), 136805.
(38) Azar, N. S.; Bullock, J.; Balendhran, S.; Kim, H.; Javey, A.; Crozier, K. B. Light−Matter Interaction Enhancement in Anisotropic 2D Black Phosphorus via Polarization-Tailoring Nano-Optics. *ACS Photonics* **2021**, *8* (4), 1120−1128.
(39) Bel Hadj Tahar, R.; Ban, T.; Ohya, Y.; Takahashi, Y. Tin doped indium oxide thin films: Electrical properties. *J. Appl. Phys.* **1998**, *83* (5), 2631−2645.
(40) Kim, H.; Pique, A.; Horwitz, J. S.; Mattoussi, H.; Murata, H.; Kafafi, Z. H.; Chrisey, D. B. Indium tin oxide thin films for organic light-emitting devices. *Appl. Phys. Lett.* **1999**, *74* (23), 3444−3446.
(41) Kioupakis, E.; Rinke, P.; Delaney, K. T.; Van de Walle, C. G. Indirect Auger recombination as a cause of efficiency droop in nitride light-emitting diodes. *Appl. Phys. Lett.* **2011**, *98* (16), 161107.
(42) Bae, W. K.; Park, Y.-S.; Lim, J.; Lee, D.; Padilha, L. A.; McDaniel, H.; Robel, I.; Lee, C.; Pietryga, J. M.; Klimov, V. I. Controlling the influence of Auger recombination on the performance of quantum-dot light-emitting diodes. *Nat. Commun.* **2013**, *4* (1), 2661.
(43) Salehzadeh, O.; Tran, N. H.; Liu, X.; Shih, I.; Mi, Z. Exciton kinetics, quantum efficiency, and efficiency droop of monolayer MoS_2 light-emitting devices. *Nano Lett.* **2014**, *14* (7), 4125−4130.
(44) Popov, A. A.; Stepanov, M. V.; Sherstnev, V. V.; Yakovlev, Y. P. 3.3-μm LEDs for measuring methane. *Tech. Phys. Lett.* **1997**, *23* (11), 828−830.
(45) Hadji, E.; Bleuse, J.; Magnea, N.; Pautrat, J. L. 3.2 μm infrared resonant cavity light emitting diode. *Appl. Phys. Lett.* **1995**, *67* (18), 2591−2593.

(46) Popov, A. A.; Stepanov, M. V.; Sherstnev, V. V.; Yakovlev, Y. P. InAsSb light-emitting diodes for the detection of CO_2 (λ = 4.3 μm). *Tech. Phys. Lett.* **1998**, *24* (8), 596−598.
(47) Popov, A. A.; Sherstnev, V. V.; Yakovlev, Y. P. Light-emitting diodes for the 1.7−2.4 μm wavelengths. *Light-Emitting Diodes: Research, Manufacturing, and Applications*; International Society for Optics and Photonics: Bellingham, WA, April 1997; Vol. *3002*, pp 132−140.
(48) Das, N. C.; Olver, K.; Towner, F.; Simonis, G.; Shen, H. Infrared (3.8 μm) interband cascade light-emitting diode array with record high efficiency. *Appl. Phys. Lett.* **2005**, *87* (4), 041105.
(49) Das, N. C. Infrared light emitting device with two color emission. *Solid-State Electron.* **2010**, *54* (11), 1381−1383.
(50) Bandyopadhyay, N.; Slivken, S.; Bai, Y.; Razeghi, M. High power, continuous wave, room temperature operation of $\lambda\sim$ 3.4 μm and $\lambda\sim$ 3.55 μm InP-based quantum cascade lasers. *Appl. Phys. Lett.* **2012**, *100* (21), 212104.
(51) Xie, F.; Caneau, C.; LeBlanc, H. P.; Visovsky, N. J.; Chaparala, S. C.; Deichmann, O. D.; Hughes, L. C.; Zah, C.-e.; Caffey, D. P.; Day, T. Room Temperature CW Operation of Short Wavelength Quantum Cascade Lasers Made of Strain Balanced GaxIn1-xAs/AlyIn1-yAs Material on InP Substrates. *IEEE J. Sel. Top. Quantum Electron.* **2011**, *17* (5), 1445−1452.
(52) Hamamatsu. *Mid Infrared LED L13454 Series*; Hamamatsu: Hamamatsu, Japan, 2017; http://www.hamamatsu.com.cn/UserFiles/upload/file/20190527/l13454_series_kled1074e.pdf (accessed Aug 1, 2021).
(53) Boston Electronics. *TE Cooled Optically Immersed 3.8 μm LED*; Boston Electronics: Brookline, MA, 2009; https://www.boselec.com/wp-content/uploads/Linear/IRSources/IRSourcesLiterature/LED38Sr.pdf (accessed Aug 1, 2021).
(54) Thorlabs. *Unmounted Single-Color LED 3800 nm*; Thorlabs: Newton, NJ, 2020; https://www.thorlabs.com/thorproduct.cfm?partnumber=LED3800W (accessed Aug 1, 2021).
(55) Abate, Y.; Akinwande, D.; Gamage, S.; Wang, H.; Snure, M.; Poudel, N.; Cronin, S. B. Recent progress on stability and passivation of black phosphorus. *Adv. Mater.* **2018**, *30* (29), 1704749.
(56) Wood, J. D.; Wells, S. A.; Jariwala, D.; Chen, K.-S.; Cho, E.; Sangwan, V. K.; Liu, X.; Lauhon, L. J.; Marks, T. J.; Hersam, M. C. Effective passivation of exfoliated black phosphorus transistors against ambient degradation. *Nano Lett.* **2014**, *14* (12), 6964−6970.
(57) Huang, S.; Zhang, G.; Fan, F.; Song, C.; Wang, F.; Xing, Q.; Wang, C.; Wu, H.; Yan, H. Strain-tunable van der Waals interactions in few-layer black phosphorus. *Nat. Commun.* **2019**, *10* (1), 2447.
(58) Huang, J.; Hou, W. J.; Li, J. H.; Li, G.; Yang, Y. Improving the power efficiency of white light-emitting diode by doping electron transport material. *Appl. Phys. Lett.* **2006**, *89* (13), 133509.
(59) Wang, X.; Xia, F. Stacked 2D materials shed light. *Nat. Mater.* **2015**, *14* (3), 264−265.
(60) Schnitzer, I.; Yablonovitch, E.; Caneau, C.; Gmitter, T. J. Ultrahigh spontaneous emission quantum efficiency, 99.7% internally and 72% externally, from AlGaAs/GaAs/AlGaAs double heterostructures. *Appl. Phys. Lett.* **1993**, *62* (2), 131−133.